An unusual * shape resonance in the near-threshold photoionization of S 1 para-difluorobenzene

Susan M. Bellm, Julia A. Davies, Paul T. Whiteside, Jingwei Guo, Ivan Powis, and Katharine L. Reid

Citation: The Journal of Chemical Physics **122**, 224306 (2005); doi: 10.1063/1.1927523
View online: http://dx.doi.org/10.1063/1.1927523
View Table of Contents: http://scitation.aip.org/content/aip/journal/jcp/122/22?ver=pdfcov
Published by the AIP Publishing

An unusual π^* shape resonance in the near-threshold photoionization of S_1 *para*-difluorobenzene

Susan M. Bellm,[a] Julia A. Davies,[b] Paul T. Whiteside, Jingwei Guo,[c] Ivan Powis,[d] and Katharine L. Reid
School of Chemistry, University of Nottingham, Nottingham NG7 2RD, United Kingdom

(Received 25 February 2005; accepted 14 April 2005; published online 13 June 2005)

Previously reported dramatic changes in photoelectron angular distributions (PADs) as a function of photoelectron kinetic energy following the ionization of S_1 *p*-difluorobenzene are shown to be explained by a shape resonance in the b_{2g} symmetry continuum. The characteristics of this resonance are clearly demonstrated by a theoretical multiple-scattering treatment of the photoionization dynamics. New experimental data are presented which demonstrate an apparent insensitivity of the PADs to both vibrational motion and prepared molecular alignment, however, the calculations suggest that strong alignment effects may nevertheless be recognized in the detail of the comparison with experimental data. The apparent, but unexpected, indifference to vibrational excitation is rationalized by considering the nature of the resonance. The correlation of this shape resonance in the continuum with a virtual π^* antibonding orbital is considered. Because this orbital is characteristic of the benzene ring, the existence of similar resonances in related substituted benzenes is discussed. © *2005 American Institute of Physics*. [DOI: 10.1063/1.1927523]

I. INTRODUCTION

Experiments in which synchrotron radiation in the uv to vuv region is used to ionize gas phase molecules are commonly used to identify and map dynamical resonances in the continuum. Such measurements of the spectra and angular distributions of photoelectrons as a function of their kinetic energy typically range from a few eV to several tens of eV above the ionization threshold.[1–3] By contrast, laser multiphoton ionization experiments, in which photoelectrons are generated close to threshold and where the ionization wavelength is usually only varied accidentally as a consequence of defining the excitation step, have rarely made reference to such resonances.[4–7] This has caused a twofold problem: (i) there is little information on resonances in the near-threshold region (where they might well be expected to appear as the interaction of the electron with the ion core is here strongest) and (ii) the unidentified presence of such resonances may affect the interpretation of the dynamics involving the prepared state that the multiphoton ionization experiments were designed to probe.

Resonances in the ionization continuum cause a large change in the phase shifts of the contributing photoelectron partial waves. Because photoelectron angular distributions (PADs) are extremely sensitive to these phase shifts[8] they are often a better indicator of the presence of a resonance than the cross section alone. As the resonance energy is passed through, the anisotropy of a PAD typically changes, giving a highly characteristic signature. A cylindrically symmetric photoelectron angular distribution $I(\theta)$ following two-photon ionization can be written as

$$I(\theta) = \beta_{00}Y_{00}(\theta,0) + \beta_{20}Y_{20}(\theta,0) + \beta_{40}Y_{40}(\theta,0), \qquad (1)$$

where the β_{20} and β_{40} coefficients are both anisotropy parameters, β_{00} is the angle-integrated cross section, and the Y_{LM} are spherical harmonics. For ease of comparison of values, and to give anisotropy parameters that depend on the shape of the PAD only, the β_{20} and β_{40} values are usually normalized by dividing by β_{00}. The resonance is then expected to show up in a plot of β_{20}/β_{00} and/or β_{40}/β_{00} versus ionization energy. When no molecular alignment is created in the excitation step, β_{40} will be zero (as it would be in the one-photon case) and $-1/\sqrt{5} \leqslant \beta_{20}/\beta_{00} \leqslant 2/\sqrt{5}$. In the one-photon case, when the precursor to ionization is not aligned, the parameter β rather than β_{20} is usually used, where $\beta = \sqrt{5}\beta_{20}/\beta_{00}$ is the coefficient of the second Legendre polynomial P_2:

$$I(\theta) \propto 1 + \beta P_2(\cos\theta). \qquad (2)$$

Para-difluorobenzene (*p*-DFB) has been well studied by spectroscopists,[9] partly because it has an easily accessible first excited state and a low ionization potential. For this reason, many studies have employed multiphoton ionization to study its spectroscopy and dynamics.[10–12] It is therefore important to understand the photoionization dynamics of *p*-DFB, particularly out of its S_1 (valence) electronic state in which a π electron is ejected. In the D_{2h} point group, which is relevant to the equilibrium structure of *p*-DFB, there are two conventions commonly found in the literature which lead to different labeling of the irreducible representations, and thus different choices of the symmetry labels describing

[a]Present address: Atomic and Molecular Physics Laboratories, Research School of Physical Sciences and Engineering, Australian National University, Canberra ACT 0200, Australia.
[b]Present address: National Physical Laboratory, Teddington, Middlesex, TW11 0LW, United Kingdom.
[c]Present address: Department of Chemistry, University of York, Heslington, York, YO10 5DD, United Kingdom.
[d]Author to whom correspondence should be addressed.

orbitals and states. These conventions place the molecule in either the *xy* or the *yz* planes with the *y* direction running perpendicular to the F–F axis in either case. We will assume the latter orientation in this paper. The effect of switching the coordinate choice is simply to interchange the $b_{1x} \leftrightarrow b_{3x}$ designations (where *x* may be either *g* or *u*).

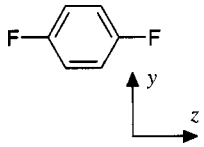

The electronic transition moment for excitation from the $S_0(^1A_g)$ ground state to the $S_1(^1B_{2u})$ excited state has b_{2u} symmetry and lies along the *y* axis. *p*-DFB has 30 nondegenerate vibrational modes which decompose into the symmetry species $6a_g+2a_u+1b_{1g}+5b_{1u}+3b_{2g}+5b_{2u}+5b_{3g}+3b_{3u}$. The $S_0(v=0) \rightarrow S_1$ excitation process allows, in principle, the formation of all totally symmetric vibrational states in S_1, but of the totally symmetric modes only modes 3, 5, and 6 (CF stretch, ring breathing, CCC in plane bend, respectively, with modes labeled using Mulliken notation) are formed with one quantum in S_1 and dominate the observed vibrational progressions. In addition, two b_{3g} modes, ν_{26} (CCC in plane bend) and ν_{27} (CF in plane bend) are weakly active as a result of vibronic coupling.[9] Excitation of one quantum in either of these modes in S_1 from $S_0(v=0)$ gives rise to a vibronic transition moment that points along *z* (i.e., the F–F direction).

In recently published work we reported a striking dependence of PADs following the ionization of $S_1(v=0)$*p*-DFB on photoelectron kinetic energy, which we tentatively attributed to a low-lying shape resonance in the continuum.[13] In this work, we demonstrate by the use of continuum multiple scattering calculations using an Xα local-exchange approximation (CMS-Xα) that a shape resonance is indeed responsible for the observed behavior. We present photoelectron spectra and angular distributions following the ionization of the prepared S_1 vibrational states $0^0(36\,838\ \mathrm{cm}^{-1})$, $5^1(0^0+815\ \mathrm{cm}^{-1})$, $5^2(0^0+1629\ \mathrm{cm}^{-1})$, $3^15^1(0^0+2065\ \mathrm{cm}^{-1})$, and $27^1(0^0+436\ \mathrm{cm}^{-1})$, and ionization with a second photon of either the same or shorter wavelength in order to examine the effects of initial and final vibrational states, and of the prepared intermediate S_1 state molecular axis alignment on the experimental PADs.

II. EXPERIMENTAL DETAILS

The apparatus has been described in detail in previous publications from this group,[12,14] here we provide a brief description and report details relevant to this work. Room temperature *p*-difluorobenzene (Aldrich, 99%) was seeded in helium and expanded through a pulsed nozzle (General Valve) into a skimmed molecular beam chamber. The skimmed molecular beam was intersected perpendicularly by a loosely focused laser beam at one end of a 24 cm long drift tube, magnetically screened by a double layer mu-metal shield. All surfaces on the inside of the drift tube were coated with graphite to minimize the build up of contact potentials and so provide an almost completely field-free environment.

The excitation laser was a pulsed Nd:YAG (YAG-yttrium aluminum garnet) (Continuum Surelite III) pumped dye laser (Continuum ND6000), the output of which was doubled and then mixed with the Nd:YAG fundamental to produce light in the range 259–271 nm which is resonant with the $S_0 \rightarrow S_1$ vibronic transitions in *p*-DFB. In the one-color experiments the same beam was used for ionization. In the two-color experiment, which was only applied when the S_1 origin transition at 271 nm was excited, a second wavelength was generated by pumping a second Continuum ND6000 dye laser with the frequency tripled output of a second Nd:YAG (Continuum Surelite I). The energy of two photons at 271 nm (9.13 eV) is less than the *p*-DFB ionization potential (9.16 eV) and so no one-color resonant ionization occurs in these experiments; the second photon wavelength was chosen to be off-resonance with any $S_0 \rightarrow S_1$ transitions and varied in the range 266 nm–225 nm. A small background signal was detected only at the shorter ionizing wavelengths and was largely due to photoemission of electrons from surfaces within the vacuum chamber with a very small contribution from single color nonresonant ionization. Thus, we observed a relatively clean two-color signal and there was no need for a background subtraction. In the one-color experiments the energy in excess of the ionization potential is defined solely by the excitation wavelength; in the two-color experiments it was chosen by selecting the wavelength of the second laser beam.

Each laser beam was passed through a zero-order half wave plate before crossing the molecular beam. The wave plates were rotated by a computer controlled stepper motor, enabling θ, the angle between the polarization vector of the ionizing light and the direction of ejection of the photoelectrons, to be varied. The angle between the polarization vectors of the synchronized excitation and ionization beams was fixed at either 0° or 90° and the polarization vectors of both beams were rotated together and with respect to the time-of-flight axis to give five angles of ejection (θ=0°, 22.5°, 45°, 67.5°, and 90°). Photoelectrons formed by (1+1) or (1+1′) resonance-enhanced two-photon ionization, and ejected along the axis of the drift tube, were detected with a 2.5 cm diameter triple microchannel plate detector (Photek) mounted at the other end, thus giving a small solid angle of detection. The photoelectron signal was passed through an amplifier (Ortec×10) and the flight times of the photoelectrons recorded with a time-to-digital converter (TDC, LeCroy 2277), which has a time resolution of 1 ns. The TDC was controlled and read by a PC via a CAMAC interface (Hytec Electronics). In order to minimize the effect of possible laser power fluctuations during the experiment, photoelectron spectra were accumulated for 1000 laser shots at each value of θ and this process was repeated at least 40 times. In addition, power-dependent studies were undertaken to ensure that the excitation step was not saturated. The photoelectron spectra were converted from their original form, as a function of photoelectron time of flight, to a function of internal energy of the *p*-DFB ion. In order to determine photoelectron angular distributions, each photoelectron peak in each spectrum was fitted to a Lorentzian function, the area

under which was taken as the peak intensity at that value of θ. The resulting $I(\theta)$ values were then fit to Eq. (1) in order to determine the anisotropy parameters.

III. THEORETICAL METHOD

The photoionization matrix elements required to compute properties such as the ionization cross sections and angular distribution parameters were obtained from CMS-Xα calculations using a methodology fully described previously.[15,16] In brief this entails, as a first step, the construction of a self-consistent ground state neutral molecule potential consisting of overlapping spherical regions centerd on each atomic site, in which the exchange contribution to an effective one-electron potential is represented using the Xα local density approximation. Electron wave functions can then be expressed in a symmetry-adapted basis of spherical harmonic functions on each center with radial terms obtained by direct numerical integration within the spherical zones of the potential.

Atomic coordinates were taken from an optimized MP2/6-31G** structure while other parameters were derived as previously described.[16] The basis functions on the atomic centers were truncated at $l_{\max}=2$ (C and F) or $l_{\max}=1$ (H), while in the spherical outer region $l_{\max}=5$ was imposed. A trial S_0 density developed with these parameters was iterated using standard techniques to obtain a self-consistent ground state potential and the associated one-electron functions.

In the present work an S_1 excited state neutral potential was then obtained from that of the S_0 ground state, modifying the electron density by the ansatz of promoting one electron from the outermost $2b_{2g}$ orbital to the $1a_u$ lowest unoccupied molecular orbital,[17] and then reiterating to achieve self-consistency while maintaining the modified occupation numbers. From these two neutral potentials we find ΔE_{SCF} for the $S_0 \rightarrow S_1$ vertical excitation is $(-430.624) - (-430.793)\mathrm{a.u.} \equiv 4.6$ eV, a value which is in excellent agreement, but probably rather fortuitously so, with the experimental transition energy (271 nm $\equiv$ 4.58 eV).

Continuum electron wave functions were subsequently calculated, and bound initial orbitals recalculated, using potentials derived directly from these converged neutral potentials, adapted to have an asymptotic Coulombic form appropriate for ion plus electron, and then photoionization matrix elements between initial and final (ionized) states were obtained[16] in a frozen core approximation ensuring orthogonality of the orbital functions. For the continuum state calculations the spherical harmonic basis expansions were extended to higher $l_{\max}$ [$l_{\max}(\mathrm{C,F})=4$, $l_{\max}(\mathrm{H})=3$, and $l_{\max}(\text{outer sphere})=8$], reflecting the expected scattering into higher l waves caused by the anisotropic ion potential. These calculations were checked for convergence in selected cases by repetition with the partial wave expansion increased to $l_{\max}(\text{outer sphere})=10$, and it was also ascertained that the bound initial levels were only minimally perturbed by the asymptotic Coulombic adaptation made to the potentials.

An initial set of calculations examined one-photon ionization from the ground S_0 state of *p*-DFB. Experimental asymmetry parameters β measured across the $\tilde{X}(2b_{2g}^{-1})$ and

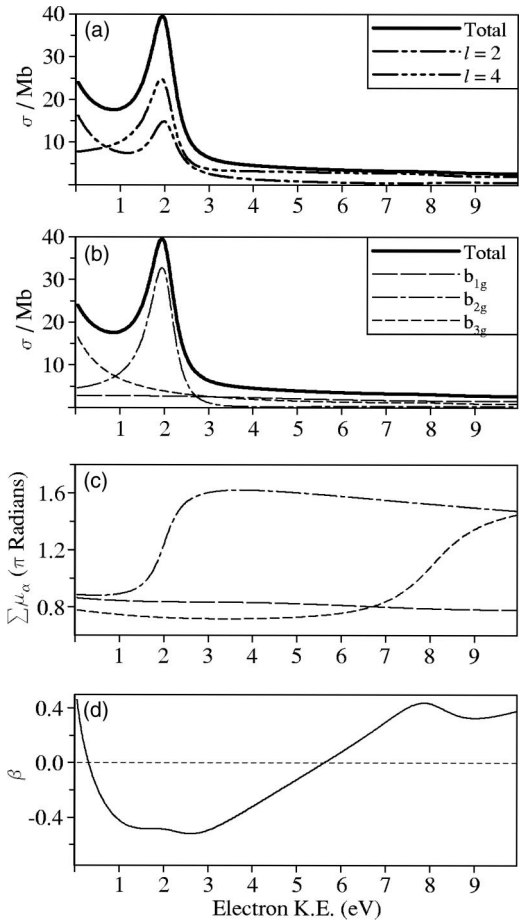

FIG. 1. CMS-Xα calculations for the $S_1\,a_u^{-1}$ photoionization: (a) cross section, decomposed into l-wave components. Higher terms ($l \geqslant 6$) make a negligible contribution and are not shown. (b) Symmetry allowed partial channel cross sections. (c) Eigenphase sums for the symmetry allowed continua [same key as (b)]. (d) β asymmetry parameter [Eq. (2)] for a randomly oriented S_1 state.

$\tilde{A}(1b_{1g}^{-1})$ photoelectron bands recorded at $h\nu=21.2$ eV have been reported,[18] and at the vertical ionization energies are reported as 0.89 ± 0.09 and 1.09 ± 0.08, respectively; these compare favorably with the corresponding values of 0.72 and 0.87 calculated here.

Having thus established that the S_0 potential provides a credible base for these calculations, further calculations were performed using the $S_1(\ldots 2b_{2g}^1 1a_u^1)$ excited state potential derived from it. In this case our treatment of the ionization dynamics needed to be extended to consider, additionally, possible alignment of the optically prepared S_1 state. For this, fixed molecule photoelectron angular distributions were calculated from the matrix elements for a specific molecular orientation[16] and these were then averaged over an appropriately weighted distribution of orientations in the lab frame to obtain predicted photoelectron angular distributions for comparison with experiment.

IV. COMPUTATIONAL RESULTS

Figure 1 shows the calculated total $S_1 a_u^{-1}$ cross section decomposed into its l-wave components and partial channel cross sections; these are the $\boldsymbol{k}b_{1g}, \boldsymbol{k}b_{2g}, \boldsymbol{k}b_{3g}$ electric dipole symmetry allowed continua. The strong peak at 2 eV above

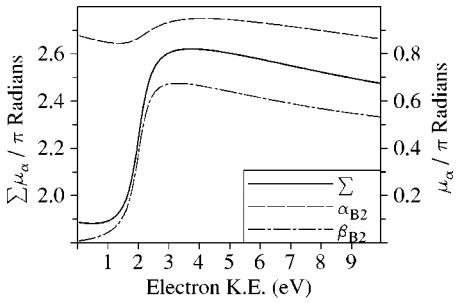

FIG. 2. CMS-Xα calculated eigenphase sum and the two most prominent individual eigenchannel phases for the b_{2g} symmetry continuum.

threshold will be identified as a shape resonance in the $\boldsymbol{k}b_{2g}$ continuum, and it can be seen that there is a corresponding dramatic dip in the calculated asymmetry parameter β [Fig. 1(d)] describing the photoelectron angular distribution from a randomly oriented S_1 state sample. Electric dipole selection rules dictate that the $\boldsymbol{k}b_{2g}$ continuum can only be directly reached by ionization of b_{1u} or b_{3u} orbitals from the S_0 state (there are no occupied a_u symmetry orbitals). Hence the first single photon S_0 ionization which might also show this same resonance behavior is then $\tilde{B}2b_{3u}^{-1}$, whose vertical ionization energy we estimate as ~14 eV.

The high molecular symmetry imposes several constraints, and consequent simplifications, for a partial wave analysis of the photoionization behavior. The inversion symmetry restricts the dipole allowed *gerade* continua to partial waves of even l only, and the b_{2g} symmetry continuum is further restricted to just odd m projections. A partial wave decomposition of the cross section into individual l waves clearly demonstrates that below 10 eV, including in the vicinity of the shape resonance, the two lowest ($l=2$ and $l=4$) waves absolutely dominate the ionization [Fig. 1(a)]. The next possible term, $l=6$, contributes less than 0.2% in this energy range.

A convenient way to visualize properties of the continuum is by using a real eigenchannel representation, obtained by diagonalization of the **K**-matrix normalized functions computed by the CMS-Xα treatment.[15,19] From this transformation one also obtains the eigenphases μ_α for each eigenchannel. The eigenphase sum,[20] $\mu_{\text{sum}}=\Sigma_\alpha\mu_\alpha$, is the multichannel analog of the single-channel central potential scattering phase shift encountered in formal scattering theory. At resonance the single-channel phase will show a rise of $\sim\pi$ rad; in the multichannel case this rise may be partially masked by changes in the nonresonant eigenchannel phase across the same region.

In the present case the eigenphase sums obtained from the calculation, Fig. 1(c), clearly confirm the dynamic resonant behavior in the b_{2g} symmetry continuum, displaying a marked rise ($\sim 0.7\pi$ rad) in the scattering phase in the region between 1 eV and 3 eV photoelectron kinetic energy, comfortably meeting established empirical criteria for the identification of a shape resonance in molecular photoionization.[21] It is also clear from examination of the individual eigenphases in the $\boldsymbol{k}b_{2g}$ continuum channel (Fig. 2) that this resonance is substantially carried by just a single eigenchannel.

Figure 3 shows contour plots of this selected resonant eigenchannel[19] which are made in a plane 0.25 Å above the molecular plane (since the latter is a nodal plane for b_{2g} symmetry) at the indicated photoelectron kinetic energies selected below, above, and at the shape resonant energy. Along with the corresponding surface representations, these show the strong localization of the continuum function around the six-membered ring *and* the enhanced amplitude that develops at resonance. These two features, of course, make for a strong overlap with the initial state wave function and so support the strongly peaked cross section at resonance, while the rapid phase change contributes also to the associated variations in the angular distribution asymmetry parameter β.

V. EXPERIMENTAL RESULTS AND DISCUSSION

Figure 4 summarizes the results presented in Ref. 13 in which the $v=0$ state in S_1 was prepared prior to ionization, and PADs were analyzed for the $v^+=0$ ion state only. A strong change in the value of β_{20}/β_{00} occurs with photoelectron kinetic energy, whereas the value of β_{40}/β_{00} remains close to zero at all energies. This variation in β_{20}/β_{00} qualitatively matches the behavior seen in the analogous β parameter calculated for an unaligned S_1 state [Fig. 1(d)], with a marked switch from a parallel to perpendicular distribution (i.e., positive to negative β parameter) within a few eV of threshold. However, the one-photon excitation of S_1 p-DFB would be expected to prepare an aligned subset of molecules in the excited state. This alignment can be characterized by a distribution of molecular axes $f(\theta)$,

$$f(\theta) = a_0 + a_2 P_2(\cos\theta), \tag{3}$$

where $P_2(\cos\theta)$ is the second Legendre Polynomial and θ is the angle between the polarization vector of the excitation laser beam and the molecular axis. The maximum possible degree of alignment induced by one-photon excitation is therefore $f(\theta)=\cos^2\theta$, or $a_2/a_0=2$.

Results of the CMS-Xα calculations described in the preceding section are included in Fig. 4 to facilitate comparison with the experimental data. Values of β_{20}/β_{00} and β_{40}/β_{00} resulting from a calculation where the maximum S_1 alignment (i.e., $a_2/a_0=2$) is assumed are shown for the six photoelectron kinetic energies studied experimentally. These calculations clearly demonstrate good agreement with experiment: small β_{40}/β_{00} values in the threshold region, but a dramatic fall and change in sign for the β_{20}/β_{00} parameters as the kinetic energy is increased. Also included in Fig. 4 is a corresponding set of calculated values of β_{20}/β_{00} obtained with the assumption of *no* intermediate S_1 alignment, i.e., $a_2=0$ (in which case β_{40} is necessarily everywhere zero, so no explicit values need be plotted). The effect of the alignment is to increase the value of β_{20}/β_{00} at all energies making for quantitative, rather than just qualitative, agreement with experiment. The calculations therefore show that the experimentally observed behavior of the PADs with photoelectron kinetic energy is indeed caused by a shape resonance in the continuum. The observed behavior of β_{40}/β_{00} is also predicted, and while this parameter value remains small

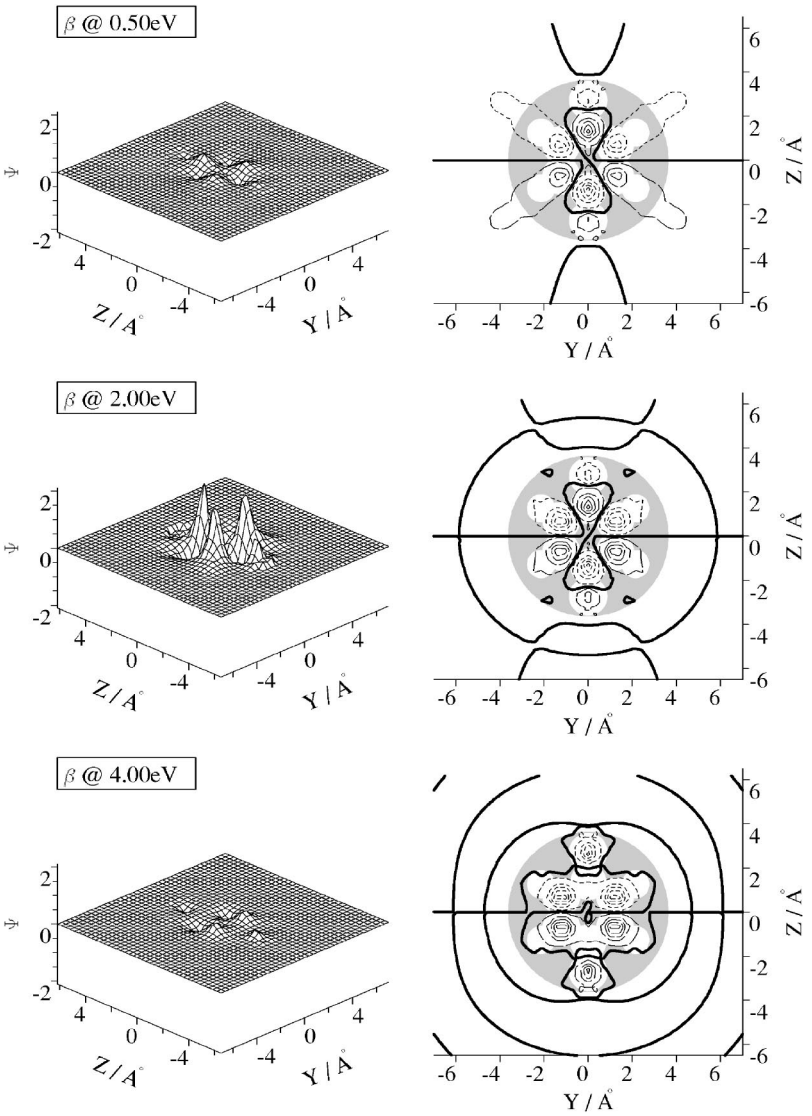

FIG. 3. Resonant eigenchannel ($\beta_{b_{2g}}$ in Fig. 2) plotted at the plane 0.25 Å above the molecular plane at selected kinetic energies below, at, and above the shape resonance energy. The surface representations (left column) are plotted with a common amplitude scale to show the increased localized amplitude at resonance. The contour plots (right column) indicate the locations of the atomic spheres and the outer sphere at their intersection with the plotting plane by shading.

there is nevertheless a clear suggestion that intermediate S_1 state alignment is important.

A direct comparison of the experimental PADs and the calculations where the full alignment, i.e., $a_2/a_0=2$, is assumed is shown in Fig. 5. However, while this particular choice of a_2/a_0 represents maximal alignment of the S_1 intermediate, in a rotationally unresolved system such as this a reduced value of $a_2/a_0=0.4$ would be predicted in the long lifetime limit, i.e., where the initially prepared alignment is reduced (but not destroyed) by molecular rotation prior to the ionization step.[22] *A priori* one might well expect this long lifetime limit to be reached in experiments such as these where nanosecond laser pulses whose duration is much longer than a rotational period have been used. Figure 5 also includes, therefore, a comparison with PADs that have been calculated for an assumed intermediate alignment of $a_2/a_0=0.4$. Clearly the agreement between calculation and experiment is actually better for $a_2/a_0=2$ than for $a_2/a_0=0.4$.

We can bring some further experimental evidence to bear on this point. We have measured PADs from S_1 *p*-DFB in experiments in which temporally overlapped laser pulses of 1 ps duration were used to excite and ionize a series of S_1 vibrational levels. In this case the laser pulse length is much shorter than a rotational period of *p*-DFB and a maximum alignment can be expected without any reduction by rotation prior to ionization. In Fig. 6 we compare the results of these picosecond laser experiments with those of our nanosecond experiments including data for all prepared S_1 and ion vibrational states, and it can be seen that the results for the two pulse durations cannot be distinguished. This therefore suggests that either the alignment produced in the two cases is the same (with the comparison with calculation suggesting it is maximal) or that the experimental PADs are completely insensitive to the extent of the intermediate state alignment.

In support of the first hypothesis, similar subnanosecond time scales for the ionization step in both experiments could be rationalized by considering the photon flux in the nanosecond pulse experiments. Taking representative pulse parameters for the ionizing laser ($\lambda=270$ nm, 3 ns pulse width, 1 mJ per pulse) and assuming that the laser beam is focused to a 100 μm spot we can estimate $I\approx 6\times 10^{27}$ photons cm^{-2} s^{-1} in the interaction region. When combined with the predicted magnitude of the ionization cross section, σ across the threshold region of $\sim$20 Mb (1 Mb$\equiv 10^{-18}$ cm^2) we obtain $\sigma I\approx 10^{11}$ s^{-1}

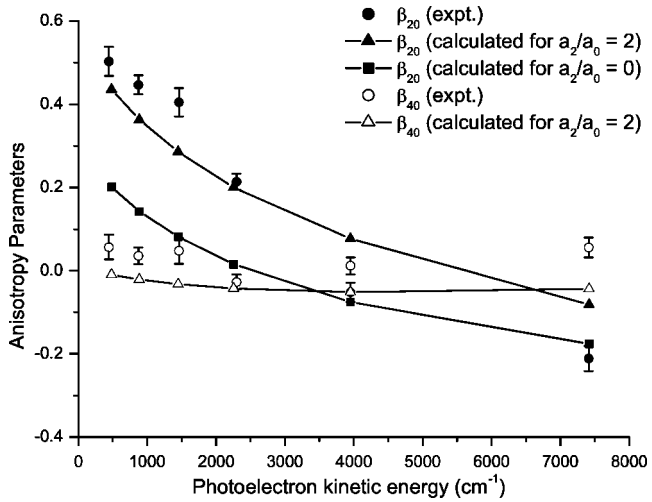

FIG. 4. Experimental and calculated normalized β_{LM} parameters describing the anisotropy of the photoelectron angular distributions following the ionization of $S_1(v=0)p$-difluorobenzene and formation of the electronic ground state of the ion in $v=0$. The solid lines joining the calculated points are to guide the eye. The six energies at which data are shown correspond to the ionizing wavelengths 266 nm, 263 nm, 259 nm, 253 nm, 244 nm, and 225 nm, and the excitation and ionization polarization vectors are parallel. The calculation is shown both for an unaligned S_1 state, and for an alignment described by $a_2=2.0$ (see text).

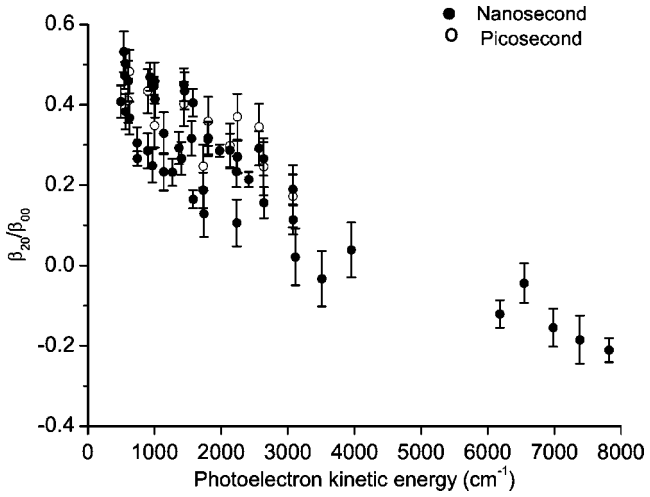

FIG. 6. Experimental normalized β_{LM} parameters describing the anisotropy of the photoelectron angular distributions following the ionization of a number of vibrational levels in S_1 p-difluorobenzene and formation of a number of (resolved) ion vibrational levels. The solid circles represent data taken when both excitation and ionization laser pulses are of ~5 ns duration and overlapped in time. The open circles represent data taken when both excitation and ionization laser pulses are of ~1 ps duration and overlapped in time. The photoelectron kinetic energy is defined by the total photon energy [$(1+1')$ or $(1+1)$] and the vibrational state formed in the ion.

molecule^{-1}, or an estimated mean lifetime of <10 ps prior to ionization, which is significantly less than the rotational period of jet-cooled p-DFB (~100 ps). These estimates assume a smooth temporal profile for the laser pulse and neglect spiking due to the mode structure of the nanosecond laser, but are sufficient to show that under the experimental conditions used the laser pulse duration is unlikely to determine directly the characteristic lifetime of the aligned intermediate state. We note that this conclusion in part relies on the comparatively large magnitude of the predicted cross section across the threshold region. Conversely, if the inference of equally strong alignment in the nanosecond and picosecond experiments is correct, it may tend to corroborate the calculation's predictions of a large magnitude cross section.

The CMS-Xα calculations thus demonstrate how the characteristics of the PADs depend on the near-threshold shape resonance, and that the quantitative comparisons (e.g., Fig. 5) may indicate a strong alignment of the intermediate S_1 state. At the same time both experimental and calculated β_{40} values remain ≈ 0. However, while a nonzero β_{40} [Eq. (1)] can only arise in at least a two-photon process where intermediate alignment is present, the converse is not true; β_{40} is not necessarily nonzero in the presence of intermediate state alignment, but rather the net anisotropy of the process can all be substantially carried in the β_{20} parameter.

However, supporting our alternative inference that the experimental PADs show little overt alignment dependence, there is an apparent lack of sensitivity to a change in the excitation-ionization laser polarization geometry. Figure 7

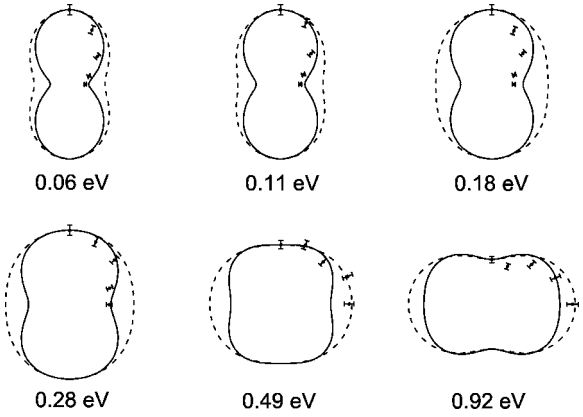

FIG. 5. Polar plots of the photoelectron angular distributions whose anisotropy parameters are given in Fig. 4. The points are experimental data points with statistical error bars going through them. The solid line is the calculated PAD for an alignment described by $a_2=2.0$ (see text). The dashed line is the calculated PAD for an alignment described by $a_2=0.4$. The $\theta=0$ direction points vertically upwards and the PADs were all normalized to give the same intensity in this direction.

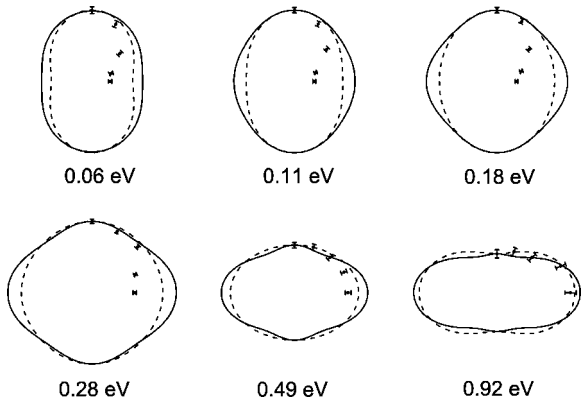

FIG. 7. As for Fig. 5 except that the polarization vectors of the excitation and ionization are fixed to be mutually perpendicular. This geometry breaks cylindrical symmetry of the resulting PAD and the measurements and calculations are taken in a plane fixed normal to the light beam directions. The θ direction points vertically upwards and is defined by the polarization direction of the ionization laser beam.

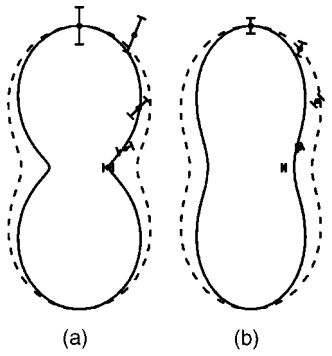

FIG. 8. Polar plots of the photoelectron angular distributions following (a) the preparation of the $6^1 S_1$ vibrational level (transition moment along z) and the formation of the 6^1 ion state and (b) the preparation of the $27^1 S_1$ vibrational level (transition moment along y) and the formation of the 27^1 ion state. In both cases the photoelectron kinetic energy is ~0.2 eV. The solid line is the calculated PAD for an alignment described by $a_2=2.0$ (see text). The dashed line is the calculated PAD for an alignment described by $a_2=0.4$.

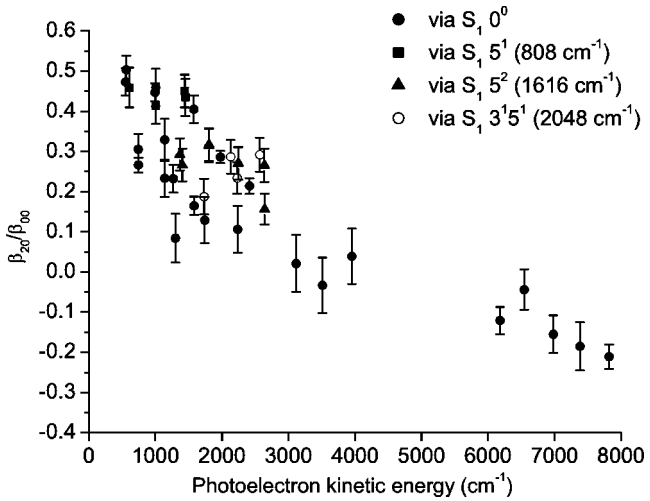

FIG. 9. As for Fig. 6 except that the data are separated out according to the prepared S_1 vibrational level. Only data taken using 5 ns laser pulses are presented.

shows measured and calculated PADs for perpendicular excitation-ionization polarization vectors. This experimental geometry breaks the cylindrical target symmetry, and these PADs are taken in a plane normal to the mutual propagation direction of the laser beams, and which contains both polarization vectors. The experimental PADs do not differ greatly from those presented in Fig. 5. While the CMS-Xα calculation again correctly predicts an effective rotation of the long axis of the PADs through 90° with increasing energy, at the quantitative level the agreement with experiment is clearly not so good as for the parallel polarization case. Nevertheless, it is also clear that the calculation does not predict a great sensitivity to intermediate alignment in this geometry, with the distinction between the results for $a_2/a_0=0.4$ and $a_2/a_0=2.0$ being insufficiently marked to permit a clear identification of the better choice.

Another opportunity to test the relative sensitivity of the experimental and calculated PADs to prepared alignment arises via the excitation of a state that is only accessible as a result of vibronic coupling. Whereas most of the "bright" S_1 vibrational levels are totally symmetric (a_g) giving a transition moment that is parallel to the pure electronic transition moment (b_{2u},y), the vibrational level with one quantum in mode 27 is active on excitation and has b_{3g} symmetry giving a b_{1u} vibronic transition moment which points along the F–F (z) direction. In Fig. 8 we show PADs resulting from the excitation of 27^1 in S_1, ionization with the same wavelength, and formation of the 27^1 level of the ion, and compare these with analogous PADs following excitation of the S_1 state 6^1 and formation of the ion state 6^1 which gives approximately the same photoelectron kinetic energy. We see that the experimental PADs are almost the same in the two cases indicating that the β_{20}/β_{00} and β_{40}/β_{00} values following excitation of 27^1 at this energy lie on the same line as all the other measured values. The corresponding results of the CMS-Xα calculations (i.e., for a pump transition moment lying along z) are also shown in Fig. 8, but these do predict changed PADs as a result of the different alignment now expected for the S_1 intermediate. Nevertheless, close comparison between the calculations and experiment for the 27^1 PAD again suggests an intermediate alignment that is significantly greater than the long lifetime limit, $a_2/a_0=0.4$, must be present.

Shape resonances in photoionization arise when the outgoing electron is temporarily trapped in the vicinity of the ion core, and one further consequence of this is enhanced electron-nuclear coupling at resonance. This is frequently manifested in non-Franck–Condon vibrational branching ratios. Because vibrational states in both the S_1 intermediate and the ion are resolved in our *p*-DFB experiments, we might expect to see some molecular vibrational dependence in our results. However, we have seen no variation of the ion vibrational branching ratios with ionization energy. This contrasts with earlier related work[4,6] in which a change in ion vibrational branching ratios has been used as a diagnostic of a resonance. We can also study how the PADs are influenced by vibrational level.[10] In Fig. 9 the dependence of β_{20}/β_{00} on photoelectron kinetic energy is distinguished according to the *intermediate* S_1 vibrational level prepared, with the data for all ion vibrational states included, while Fig. 10 shows an analogous plot when all S_1 vibrational levels are included but the data are distinguished according to *final ion* vibrational

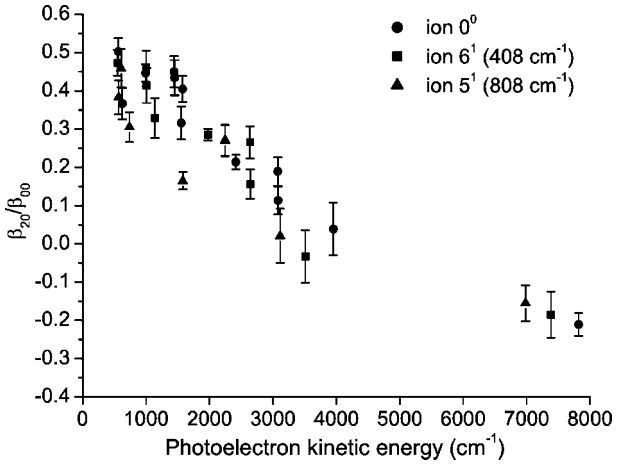

FIG. 10. As for Fig. 9 except that the data are separated out according to the ion vibrational state formed.

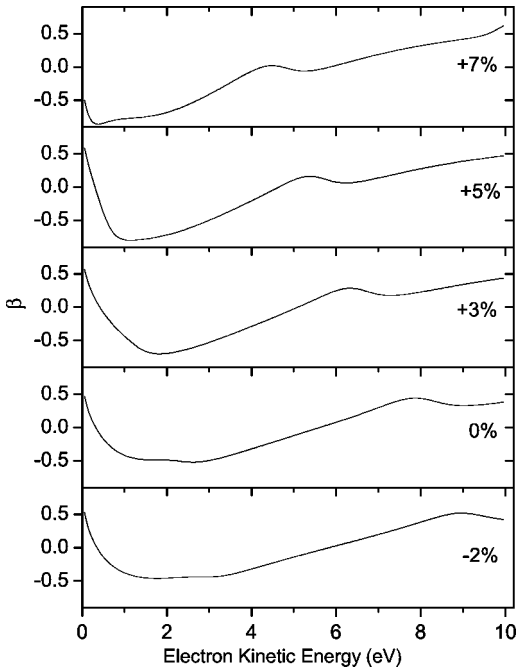

FIG. 11. Calculated β asymmetry parameters showing the sensitivity of the photoelectron angular distributions to the indicated rescaling of the assumed molecular bond lengths. (See text.)

level. It can be seen that in both cases there is little, if any, dependence of the PAD on vibrational level, other than the associated dependence on photoelectron kinetic energy. Again, this vibrational independence of the PADs contrasts with other examples in the literature.[5,6,23]

In common with other approaches to the treatment of molecular photoionization dynamics,[6,24] the CMS-Xα calculations do not explicitly include any effects of vibrational motion, being performed for a fixed nuclear configuration. However, insight can be gained by performing calculations for several fixed geometries, spanning the range of the vibrational motion. In Fig. 11 we show the variation of the asymmetry parameter β (typifying the behavior of the photoelectron angular distributions) as *all* the *p*-DFB bond lengths are scaled up and down by a few percent. Although not corresponding to an exact normal mode, this allows us to examine the behavior under symmetrical breathing-type motions of the molecule. In these investigations it is found that although the $\boldsymbol{k}b_{2g}$ shape resonance shifts downwards in energy from 3 to 0.5 eV with increasing bond length, the angular distribution is, at least qualitatively, little affected. In fact a far more dramatic change is seen in the shift of a small dip in the β curve which in Fig. 11 starts at >10 eV and moves down to 5 eV. This dip is associated with a $\boldsymbol{k}b_{3g}$ shape resonance that can be seen from the eigenphase sum analysis at 9 eV in Fig. 1(c). Its rather typical behavior serves to underline the relative insensitivity of the $\boldsymbol{k}b_{2g}$ resonance to movement of the nuclei in the molecule.

In seeking to understand this insensitivity to vibrational motion it is instructive to consider more closely the nature of the $\boldsymbol{k}b_{2g}$ shape resonance. As can be seen in Fig. 3 there is comparatively little density on the fluorine atoms in this resonant eigenchannel until above the resonance energy, and at the resonance energy itself we note there is some semblance of a sixfold symmetry reminiscent of a π^* orbital in the isolated benzene ring. Repeating the above exercise, but varying only the C–F bond lengths produces even less change in the predicted angular distributions, thus emphasizing the association of the resonance with the benzene ring structure. It is also then clear that this resonance does not result from electron trapping in an inner-well potential created between the electronegative fluorine atoms, as is sometimes postulated in heavily fluorinated species.[25]

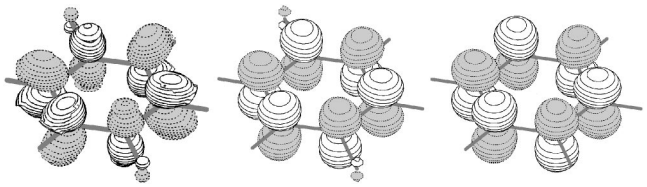

FIG. 12. Left: CMS-Xα $\boldsymbol{k}b_{2g}$ resonant eigenchannel (see Fig. 3) at the *p*-DFB shape resonance. Center: HF/STO-3g $3b_{2g}$ virtual π^* orbital of *p*-DFB Right: HF/STO-3g $1b_{2g}$ virtual π^* orbital in benzene.

A more qualitative approach to understanding shape resonances than the electron scattering calculation undertaken here seeks to identify them with excitations to virtual valencelike antibonding orbitals which are embedded in the continuum.[26,27] The $3b_{2g}$ π^* orbital of *p*-DFB is the lowest lying virtual orbital of gerade symmetry obtained in minimal basis calculations. This includes both the conventional HF/STO-3G (HF—Hartree–Fock) calculation for the S_0 ground state of *p*-DFB, and also a HF level calculation for the S_1 excited neutral state, performed using the maximum overlap method (MOM) implemented in Q-Chem[28] to maintain the $\ldots 2b_{2g}^1 a_u^1$ excited intermediate configuration.

Figure 12 compares a three-dimensional (3D) isosurface representation of the real resonant eigenchannel with that of the HF $3b_{2g}$ virtual orbital and of the analogous $1b_{2g}\pi^*$ virtual orbital of benzene. The correspondence between these pictorial representations of the *p*-DFB resonance and a π^* orbital is obvious, but while this seemingly corroborates a received wisdom, there are few systematic studies, to our knowledge, to validate this approach other than as a tool for *post hoc* rationalization in such cases as this. However, one such investigation of nine *linear* molecules[26] concluded that "the lowest π^* virtual orbital always corresponds to discrete uv transitions, and not to resonances in the continuum," in stark contrast with what is shown here for *p*-DFB. The more familiar σ-type resonances naturally concentrate electron density between nuclei, the scattering from which then readily provides a sensitivity to the internuclear spacing due to interference effects with the backscattered waves, and which can greatly influence the PADs.[29] Here, however, it can be seen that the π^* characteristic of the $\boldsymbol{k}b_{2g}$ resonance by contrast removes electron density from the internuclear regions, and thus we can rationalize a much reduced sensitivity of the PADs to the C–C bond lengths in such cases. A similar reasoning has been invoked to explain the insensitivity to internuclear separation displayed in a theoretical study[30] of the $\boldsymbol{k}\pi_u$ shape resonance in Cl_2.

In one of the few previous cases where a polyatomic molecule π^* shape resonance has been experimentally studied with vibrational resolution, the ionic state vibrational

TABLE I. Hartree–Fock minimal basis (STO-3G) virtual π^* orbital eigenvalues and corresponding estimated photoionization shape resonance energies.

Molecule	π^*virtual orbital symmetry	Eigenvalue (hartrees)	Resonance energy[a] (eV)
Benzene	b_{2g}	0.509 11	3.50
Chlorobenzene	b_1	0.481 49	2.92
Fluorobenzene	b_1	0.495 05	3.20
p-diFluorobenzene (S_0)	b_{2g}	0.487 75	3.05
p-diFluorobenzene (S_1)	b_{2g}	0.458 00	2.42
1,3,5 triFluorobenzene	a_2''	0.480 12	2.89

[a]Estimate from HF eigenvalues using the correlation given in Ref. 26.

branching ratio for CS_2 was shown to be nearly constant across the resonant excitation region,[31] which carries the implication that the shape resonant ionization dynamics are not sensitive to molecular geometry. This corroborates theoretical predictions for this resonance which identifies an atomic-like nature of the $\boldsymbol{k}\pi$ resonant state, having the character of S atom *d* functions.[32] This explanation for CS_2 therefore invokes the strong localization of the resonance at the extremities of the molecule to explain the vibrational insensitivity, in contrast to the present case where the resonant state is strongly delocalized around the ring.

The question may be posed whether the analogous ring π^* virtual orbitals in other substituted benzenes might also correspond to shape resonances in the ionization of those systems. Table I presents the minimal basis HF/STO-3G π^* virtual orbital eigenvalues for a number of such molecules. Such unoccupied virtual orbital energies are not subjected to variational improvement in the normal course of a HF calculation, but nevertheless they are seen to be very similar for these molecules. These eigenvalues may be expected to overestimate the energy of a corresponding state embedded in the ionization continuum, since the removal of an electron on ionization would undoubtedly lead to a relaxation and consequent lowering of the energy. Using an empirical correlation[26] established for linear molecules, suggests that corresponding shape resonances would be seen in the region around 3 eV above threshold, as indeed found for *p*-DFB.

In the core level excitation spectrum of gaseous benzene the $b_{2g}\,\pi^*$ feature is observed as a discrete excitation some 1.4 eV *below* the C 1*s* edge (although in condensed phase samples the C 1*s* binding energy is shifted such that the $b_{2g}\,\pi^*$ excitation does now fall in the above-edge continuum).[33] There is, however, a known tendency for resonances observed in core ionization to be shifted by a few eV to lower kinetic energy due to interaction with the core hole, so that π^* shape resonances might still be expected in valence shell ionization. However, in the high symmetry (D_{6h}) of benzene, dipole selection rules determine that a b_{2g} continuum can only be accessed by ionization of b_{1u} or e_{2u} orbitals, and the only pertinent valence shell ionization is thus $2b_{1u}^{-1}$. While other valence ionizations in benzene display clear evidence of an $e_{1u}\,\sigma^*$ shape resonance in the asymmetry parameters that for the $2b_{1u}$ orbital has no discernible structure.[2] Even the most recent single center expansion B-spline density functional theory calculations[24,34] give relatively poor agreement with these experimental β parameters in the critical region up to 20 eV above threshold. These calculations do not, however, predict a $b_{2g}\,\pi^*$ resonance feature, but it may be noted that they suffer a systematic shift to low energy (due to the attractiveness of the potential used and incomplete treatment of screening response effects) such that any resonances expected within only a few eV above the ionization threshold may be "lost" as they are shifted below threshold. Thus the existence of a $b_{2g}\,\pi^*$ shape resonance in the valence shell ionization of benzene remains inconclusive.

The analogous π^* virtual orbital in the C_{2v} monosubstituted halobenzenes is of b_1 symmetry. Photoelectron asymmetry parameters of chlorobenzene have been measured over an extended energy range, but with particular attention focusing on a Cooper minimum at $h\nu \approx 40$ eV.[3] Because of this interest the data are a little sparse in the threshold region, but the $6b_2^{-1}\beta$ parameter curve displays a very sharp feature at ~6 eV kinetic energy. However, the $b_2 \rightarrow b_1$ excitation is dipole forbidden and a CMS-Xα calculation we have performed allows the identified feature to be assigned to a $\boldsymbol{k}a_1$ shape resonance. For the other bands, although an eigenphase analysis suggests a weak $\boldsymbol{k}b_1$ shape resonance at threshold, neither the calculations nor the experimental data provide any unambiguously assignable structure in the relevant region.

In contrast, CMS-Xα calculations for fluorobenzene (C_{2v}) suggest that here a $\boldsymbol{k}b_1$ shape resonance may be discernible at ~4 eV kinetic energy, and an eigenchannel analysis reveals a very similar ring π^* character for this resonance. Even more markedly, such calculations suggest that for 1,3,5-trifluorobenzene (D_{3h}) pronounced structure in the cross section and asymmetry parameter should result from a $\boldsymbol{k}a_2''$ shape resonance at 3–4 eV kinetic energy, and an eigenchannel examination again shows the ring π^* antibonding orbital character of the resonant state. In neither case are we aware of relevant experimental data. It would thus be of some interest to perform further near-threshold ionization experiments for various fluorobenzenes to ascertain whether they also display ring π^* shape resonant features analogous to that of *p*-DFB demonstrated by the present results.

In conclusion, the CMS-Xα calculations demonstrate that a rather unusual shape resonance is responsible for the observed behavior in the two-photon ionization of *p*-DFB via the S_1 state. The prominence of the resonant behavior seen in the photoelectron angular distribution is a consequence of the high symmetry which greatly restricts the relevant continuum and its partial wave expansion. Unlike many other multichannel molecular systems the phase shift at resonance is not greatly masked by a nonresonant phase rise contributed by many other channels, allowing a clear manifestation of the resonance in the phase sensitive angular distributions. The nature of the resonance, with its concomitant lack of sensitivity to bond length, means that these fixed geometry calculations give results that compare remarkably well with the experimental data. These calculations also hint at the existence of a strong intermediate state alignment, while demonstrating that such alignment may not necessarily be so simply manifested as was perhaps anticipated. In particular, the assumption of a strong S_1 alignment does not here sig-

nificantly increase above zero the second angular distribution parameter β_{40} (which paradoxically could only take nonzero values because of intermediate alignment effects) but it does make more quantitative the experimental-theoretical agreement in the original β_{20} parameter values. Nevertheless, the particular challenges associated with calculating the photoelectron dynamics near threshold in general, and at resonance in particular, where the photoelectron scattering should be at its most sensitive, mean that fully quantitative agreement cannot be achieved and leaves open some questions relating to the intermediate state alignment effects.

The apparent correlation of shape resonances with virtual orbitals means that other related molecules may display similar behavior, and this underlines the need for more near-threshold energy-dependent studies to be carried out. This is particularly important in cases when the analysis of data relies on the assumption that the continuum function varies only very slowly with energy.

ACKNOWLEDGMENTS

K.L.R. acknowledges EPSRC for funding Grant Nos. GR/M83759 and GR/R72297, including postdoctoral support for J.A.D. and S.M.B. Support for performing *p*-DFB geometry optimizations was provided by the EPSRC National Service for Computational Chemistry Software. The authors thank Nick Besley for providing the Q-Chem MOM calculation for S_1 *p*-DFB, and Stephen Pratt for comments on these virtual orbitals and the shape resonance.

[1] J. B. West, J. Electron Spectrosc. Relat. Phenom. **68**, 233 (1994).
[2] P. Baltzer, L. Karlsson, B. Wannberg, G. Ohrwall, D. M. P. Holland, M. A. MacDonald, M. A. Hayes, and W. von Niessen, Chem. Phys. **224**, 95 (1997).
[3] A. W. Potts, D. Evardsson, L. Karlsson *et al.*, Chem. Phys. **254**, 385 (2000).
[4] P. J. Miller, L. P. Li, W. A. Chupka, and S. D. Colson, J. Chem. Phys. **89**, 3921 (1988).
[5] P. J. Miller, W. A. Chupka, J. Winniczek, and M. G. White, J. Chem. Phys. **89**, 4058 (1988).
[6] M. Braunstein, J. A. Stephens, and V. McKoy, J. Chem. Phys. **90**, 633 (1989).
[7] J. A. Stephens, M. Braunstein, and V. McKoy, J. Chem. Phys. **92**, 5319 (1990).
[8] K. L. Reid, Annu. Rev. Phys. Chem. **54**, 397 (2003).
[9] A. E. W. Knight and S. H. Kable, J. Chem. Phys. **89**, 7139 (1988).
[10] E. Sekreta, K. S. Viswanathan, and J. P. Reilly, J. Chem. Phys. **90**, 5349 (1989).
[11] G. Reiser, D. Rieger, T. G. Wright, K. Muller-Dethlefs, and E. W. Schlag, J. Phys. Chem. **97**, 4335 (1993); M. Fujii, T. Kakinuma, N. Mikami, and M. Ito, Chem. Phys. Lett. **127**, 297 (1986).
[12] K. L. Reid, T. A. Field, M. Towrie, and P. Matousek, J. Chem. Phys. **111**, 1438 (1999).
[13] S. M. Bellm and K. L. Reid, Phys. Rev. Lett. **91**, 263002 (2003).
[14] D. Townsend and K. L. Reid, J. Chem. Phys. **112**, 9783 (2000).
[15] I. Powis, J. Chem. Phys. **103**, 5570 (1995).
[16] P. Downie and I. Powis, J. Chem. Phys. **111**, 4535 (1999).
[17] O. Gunnarsson and B. I. Lundqvist, Phys. Rev. B **13**, 4274 (1976).
[18] J. A. Sell, D. M. Mintz, and A. Kuppermann, Chem. Phys. Lett. **58**, 601 (1978).
[19] D. Loomba, S. Wallace, D. Dill, and J. L. Dehmer, J. Chem. Phys. **75**, 4546 (1981).
[20] A. U. Hazi, Phys. Rev. A **19**, 920 (1979); J. Macek, *ibid.* **2**, 1101 (1970).
[21] W. Thiel, J. Electron Spectrosc. Relat. Phenom. **31**, 151 (1983).
[22] R. N. Zare, Ber. Bunsenges. Phys. Chem. **86**, 422 (1982).
[23] M. Braunstein and V. McKoy, J. Chem. Phys. **90**, 2575 (1989).
[24] M. Stener, S. Furlan, and P. Decleva, Phys. Chem. Chem. Phys. **3**, 19 (2001).
[25] J. L. Dehmer, J. Phys. Chem. **56**, 4496 (1972).
[26] J. Kreile, A. Schweig, and W. Thiel, Chem. Phys. Lett. **108**, 259 (1984).
[27] J. A. Sheehy, T. J. Gil, C. L. Winstead, R. E. Farren, and P. W. Langhoff, J. Chem. Phys. **91**, 1796 (1989).
[28] J. Kong, C. A. White, A. I. Krylov *et al.*, J. Comput. Chem. **21**, 1532 (2000).
[29] Y. Hikosaka, J. H. D. Eland, T. M. Watson, and I. Powis, J. Chem. Phys. **115**, 4593 (2001).
[30] M. Braunstein and V. McKoy, J. Chem. Phys. **92**, 4887 (1990).
[31] S. Kakar, H. C. Choi, and E. D. Poliakoff, J. Chem. Phys. **97**, 4690 (1992).
[32] R. E. Stratmann and R. R. Lucchese, J. Chem. Phys. **101**, 9548 (1994).
[33] J. A. Horsley, J. Stohr, A. P. Hitchcock, D. C. Newbury, A. L. Johnson, and F. Sette, J. Chem. Phys. **83**, 6099 (1985).
[34] M. Venuti, M. Stener, and P. Decleva, Chem. Phys. **234**, 95 (1998).